INSTITUTE OF PHYSICS PUBLISHING PLASMA PHYSICS AND CONTROLLED FUSION

Plasma Phys. Control. Fusion **46** (2004) B143–B155 PII: S0741-3335(04)83187-7

The dynamic ergodic divertor in the TEXTOR tokamak: plasma response to dynamic helical magnetic field perturbations

K H Finken[1], S S Abdullaev[1], W Biel[1], M F M de Bock[2], C Busch[1], E Farshi[2], M von Hellermann[2], G M D Hogeweij[2], M Jakubowski[1], R Jaspers[2], H R Koslowski[1], A Kraemer-Flecken[1], A Lazaros[2], M Lehnen[1], Y Liang[1], A Nicolai[1], O Schmitz[1], B Unterberg[1], E Westerhof[2], R Wolf[1], O Zimmermann[1], M de Baar[2], G Bertschinger[1], S Brezinsek[1], I G J Classen[2], A J H Donné[2], H G Esser[1], H Gerhauser[1], B Giesen[1], D Harting[1], J A Hoekzema[1], P W Huettemann[1], S Jachmich[3], K Jakubowska[2], D Kalupin[1], F Kelly[1], Y Kikuchi[5], A Kirschner[1], R Koch[3], M Korten[1], A Kreter[1], J Krom[1], U Kruezi[1], A Litnovsky[1], X Loozen[1], N J Lopes Cardozo[2], A Lyssoivan[3], O Marchuk[1], Ph Mertens[1], A Messiaen[3], O Neubauer[1], V Philipps[1], A Pospieszczyk[1], D Reiser[1], D Reiter[1], A L Rogister[1], T Van Rompuy[4], A Savtchkov[1], U Samm[1], R P Schorn[1], F C Schueller[2], B Schweer[1], G Sergienko[1], K H G Telesca[4], M Tokar[1], G Van Oost[4], R Uhlemann[1], G Van Wassenhove[3], R Weynants[3], S Wiesen[1] and Y Xu[3]

[1] Trilateral Euregio Cluster: Institut für Plasmaphysik, Forschungszentrum Jülich GmbH, EURATOM Association, D-52425 Jülich, Germany
[2] FOM Institute for Plasma Physics Rijnhuizen, Association EURATOM-FOM, PO Box 1207, NL-3430 BE Nieuwegein, The Netherlands
[3] Laboratoire de Physique des Plasmas/Laboratorium voor Plasmafysica, ERM/KMS, EURATOM Association, B-1000 Brussels, Belgium
[4] Department of Applied Physics, Ghent University, Rozier 44, B-9000 Ghent, Belgium
[5] Department of Energy Engineering and Science, Graduate School of Engineering, Nagoya University, Japan

Received 2 July 2004
Published 17 November 2004
Online at stacks.iop.org/PPCF/46/B143
doi:10.1088/0741-3335/46/12B/013

Abstract

Recently, the dynamic ergodic divertor (DED) of TEXTOR has been studied in an $m/n = 3/1$ set-up which is characterized by a relatively deep penetration of the perturbation field. The perturbation field creates (a) a helical divertor, (b) an ergodic pattern and/or (c) excitation of tearing modes, depending on whether the DED current is static, rotating in the co-current direction or in the counter-current direction. Characteristic divertor properties such as the high recycling regime or enhanced shielding have been studied. A strong effect of the ergodization is spin up of the plasma rotation, possibly due to the electric field at the plasma edge. Tearing modes are excited in a rather reproducible

way and their excitation threshold value, their motion and their reduction due to the ECRH/ECCD have been studied. The different scenarios are characterized by strong modifications of the toroidal velocity profile and by a reduced or enhanced radial transport.

(Some figures in this article are in colour only in the electronic version)

1. Introduction

The original aim of the dynamic ergodic divertor (DED) design was to spread the heat over a large area of the divertor target plate. For this reason, an ergodic divertor was selected as the base concept with similar properties to those of previous ergodization experiments [1–6]. The ergodization should 'weave' the magnetic field lines at the plasma boundary, thereby enhancing the radial heat and particle transport. The enhanced radial transport increases the scrape-off-layer width and enlarges the deposition pattern. In addition, as a new feature, the ergodic divertor was chosen to be dynamic, which means the power deposition pattern is swept toroidally by a rotation of the external perturbation field.

However, the analysis of the magnetic field line structure showed rather quickly that the assumption of an ergodic zone reaching to the target plate is an oversimplification. Indeed, only a few magnetic field lines reach from the ergodic zone towards the wall; the majority of the field lines near the wall are dominated by the near field of the perturbation current and show a relatively short connection length between two intersections with the wall. They have basically similar properties as the field lines of the scrape-off-layer, however, complicated by the fact that some field lines have a connection length corresponding to one poloidal turn and others with multiples of this length. The field lines with similar connection lengths form continuous areas and have sharp boundaries with respect to those of different connection lengths. The set of these field lines is called a laminar zone and, just as for a stellarator, one has to apply a three-dimensional model for the transport [7–13].

In its lowest frequency operation, the DED is laid out to sweep the power over the large area of the target plate. However, we have also foreseen rotation frequencies up to the diamagnetic drift frequency and hope to obtain new physics scenarios. The perturbation coil set-up is flexible enough to either allow a deep penetration of the field into the plasma or to restrict the DED field to the boundary. Together with the dynamic option, this gives a very high degree of flexibility.

In this paper we will present the results of the $m/n = 3/1$ set-up of the DED with the deep field penetration. After a description of the DED, we will first treat some divertor properties imposed by the near field of the DED. In the next section the action of the ergodization will be discussed. The deep penetration of a resonant magnetic perturbation excites tearing modes in a reproducible way in the plasma. Properties of the tearing modes and resulting effects are discussed next. Finally, we discuss transport measurements of the different scenarios and their confinement.

2. The set-up of the DED

The main component of the DED is a set of coils to perturb the edge magnetic fields as shown in figure 1; these coils are located inside the vacuum vessel at the high field side of the torus [14]. The set consists of 16 coils (four quadruples) plus two compensation coils. The individual

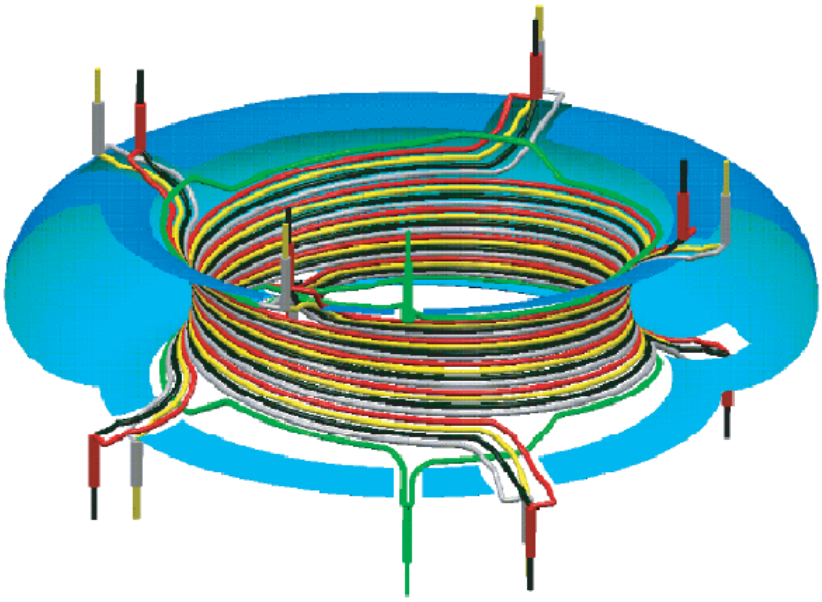

Figure 1. Schematic set-up of the DED coils at the TEXTOR tokamak. The coils are wound helically at the high field side of the torus inside the vessel. The coils are essentially parallel to the magnetic field lines of the plasma edge.

perturbation coils follow the direction of the equilibrium magnetic field of the plasma edge (i.e. helically) once around the torus; the radial location of enhanced interaction where the helical pitch of the coils exactly matches that of the equilibrium field can be fine-tuned, e.g. by varying the plasma current.

The feeders of all coils are brought to the outside of the vessel such that they can be interconnected in arbitrary ways. The two important set-ups used so far are the $m/n = 12/4$ configuration and the $m/n = 3/1$ configuration. In the $12/4$ configuration, neighbouring coils are supplied with a phase difference of 90° (AC-mode of operation) such that a relatively fine structured rotating perturbation field is excited. In the $3/1$ set-up four coils are switched in parallel and neighbouring quartets form a much coarser rotating field pattern. The high multipolarity of the set-up restricts the perturbation field to the very edge of the plasma while the low polarity provides a deep penetration of the DED field into the plasma.

For the AC operation we can select two scenarios, the so-called co-rotation and counter-rotation. Co-rotation means that the toroidal projection of the DED field rotation would excite a rotation in the direction of the plasma current; at the same time, the projection in the poloidal direction is that of the ion drift direction. Counter-rotation (ctr-rotation) has the opposite sense.

3. The helical divertor

The divertor is generated by the superposition of the equilibrium field and the near field of the DED. Since the external coils are aligned nearly parallel to the magnetic field lines in the outer part of the plasma, the radial component of the DED field acts over a long distance on the same field line and thus produces a relatively large displacement of the field line. Because of this spatial resonance, a helical configuration such as the DED requires the lowest external current of all divertor configurations to produce an X-point [15, 16]. It needs about half an

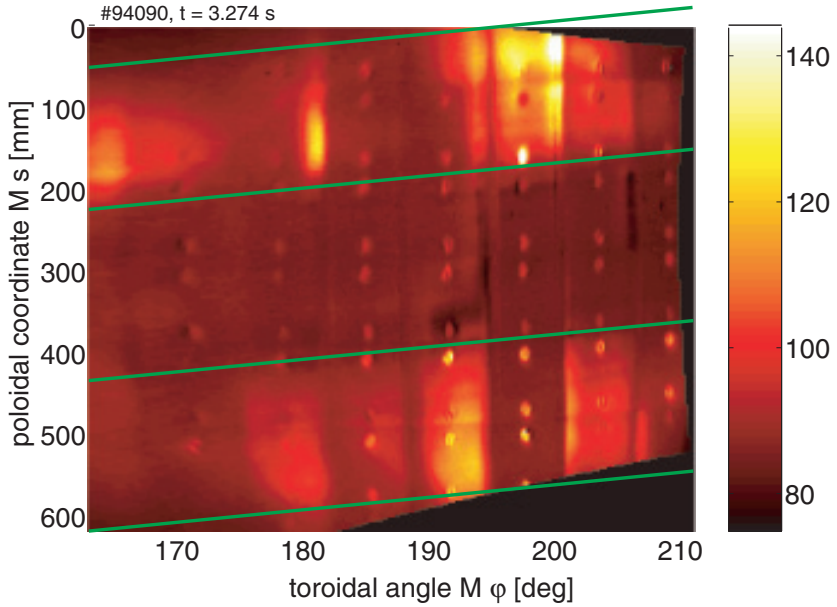

Figure 2. Thermographic recording of the surface temperature of the static divertor given by the near field of the DED. The lines guide the eye along the helical stripes.

order of magnitude less current than the conventional poloidal divertor. Since the TEXTOR design uses a continuous coil winding for the DED, instead of modules such as have been used in previous experiments, a smooth helical divertor structure is formed.

Local measurements of power deposition and recycling together with probe measurements serve to delineate the divertor properties. One of the original aims of the DED experiment is the distribution of the heat on the target plates. Figure 2 shows the heating pattern recorded by an IR camera; for this image, the DED is working in the $m/n = 3/1$ configuration, already mentioned before. One sees clearly the graphite tiles and the tightening screws. The image of the curved and oblique surface is corrected such that the tiles form a regular pattern; this correction explains the deformed boundary of the image. It is obvious that the helical heating stripe has a slight slope from the bottom left to the right; the stripe follows the direction of the DED coils behind the target plate. The colour represents the temperature as indicated by the colour bar at the right. Unfortunately, the tiles are not ideally mounted and, as a result, the protruding edges of the graphite tiles receive an enhanced heat flux.

Figure 3 shows a sequence of temperature distributions for the operation of the DED at 1 kHz. The images are recorded every 115 μs; at this high recording frequency, the recorded area has to be reduced to a rectangle of 32 mm $\times$ 256 mm (16 $\times$ 128 pixel). The sequence corresponds to one period of the DED current. Despite the rapid rotation, one still sees the footprints of the heat, when the strike point hits the target in the observation area. The difference between the hottest (red) and coldest (blue) parts amounts to 10° and the ratcheting of the temperature during the 2 s long application of the DED amounts also to only 10–20°. The observation shows clearly, that (a) the instantaneous heat deposition patterns in static and 1 kHz operation are similar and (b) that the envisaged heat distribution by the DED works as planned.

The divertor shape is nicely represented by a tangential view in TEXTOR in CIII line radiation as shown in figure 4. The field structure, obtained from Poincaré mapping, is

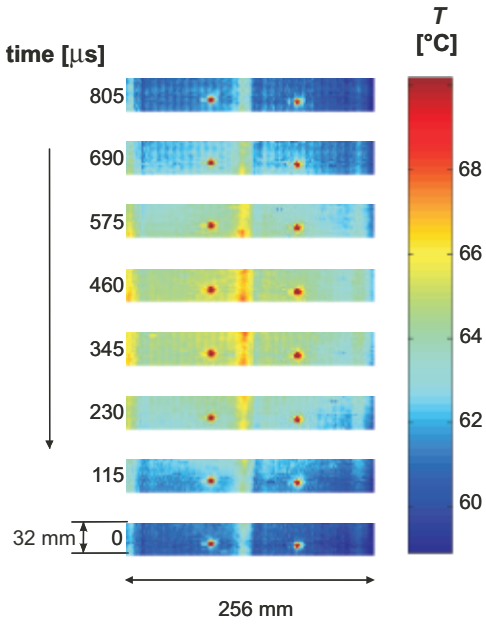

Figure 3. Sequence of thermographic snapshots with short exposure times for the DED divertor operating at a frequency of 1 kHz. The images show clearly the modulation of the instantaneous heat flux, even at a rotation frequency of 1 kHz.

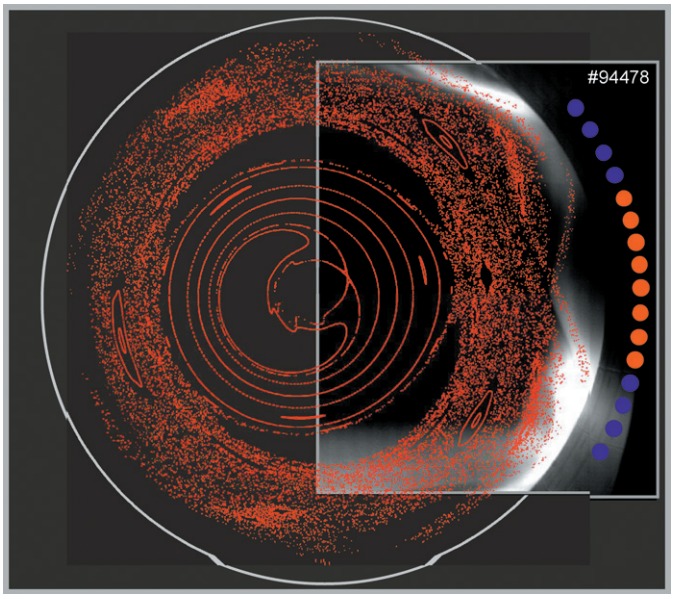

Figure 4. Divertor structure in the light of CIII; superimposed are the structures obtained from Poincaré mapping. One recognizes the similarities in the recycling structures and the field line structures. On the right, the DED coils are indicated; the two colours represent the directions of the electric current. The maximum total current per mode amounts to 30 kA.

superimposed on the image. One sees clearly the two strike zones on the right and on top and, at high density, the two strike zones connected to the X-point. The structures of the CIII recycling light reveal many details of the structures in the Poincaré plot. High density discharges with static DED tend to the formation of MARFEs near the X-point in a similar way to poloidal divertors. MARFE generation is strongly suppressed for the rotating DED-field [17]. More details of the divertor properties have been presented at the recent PSI conference [18]. Many similarities between conventional and helical divertors of the DED have been shown, such as the high recycling regime and the efficient screening of impurities.

4. Properties resulting from ergodization

When the DED is applied, two different states are obtained: one is attributed to the ergodization and the other results from the excitation of a tearing mode. The two different states can be selected by the operation of the DED. The ergodization dominated scenario is obtained at low DED coil currents (typically $I_{\mathrm{DED}} < 0.6$ kA per coil) or for the co-rotating DED field up to the highest amplitudes. The tearing mode dominated scenario occurs for static and ctr-rotating DED beyond a rather reproducible threshold value. Only very few discharges with a co-rotating DED field show mode activation; discharges are described in this section without tearing mode excitation.

The ergodization results from the superposition of the equilibrium magnetic field and the resonant external DED field. It consists of the proper ergodic zone where an enhanced radial transport is expected and the laminar zone, where field lines intersect the wall. In the latter zone, transport is dominated by mobile electrons and ions, which, due to ambipolarity constraints, establish an electric field. Due to the high electrical conductivity, the field pattern is transported into the ergodic zone, creating a highly complicated field structure. It is expected that effects based on ergodization grow monotonically with the current in the DED coils. We observe modifications of the modes and of the turbulence spectrum. However, the strongest effect is an acceleration of the plasma rotation. The toroidal plasma rotation is measured by charge exchange recombination spectroscopy, CXRS, using the co-NBI of TEXTOR [19]. The NBI is equipped with a graphite V-target which limits the height of the neutral beam; by choosing a small 4 cm wide opening of the V-target, it is possible to obtain sufficient light for CXRS while minimizing the additional power and momentum input from the beam. Figure 5 shows the development of the toroidal velocity profile for a discharge with co-rotating DED at a frequency of 1 kHz. The radial axis is normalized. Unfortunately, our CXRS-system only allows detection over the inner $2/3$ of the minor radius. The units of the velocity are rad s^{-1}; in order to obtain the velocity, the value has to be multiplied by the major radius ($R_0 = 1.75$ m, $a = 0.46$ m). For the given discharge, all parameters are constant in the interval from 1 to 4 s; only the DED current is ramped up starting at 1 s, reaching its maximum at 2.5 s, keeping the amplitude constant to 3 s and ramping down to 3.2 s.

The figure shows clearly that the toroidal plasma velocity grows by the same amount at all radial locations. The spin-up of the plasma is quite substantial, as compared with the rotation prior to the DED onset. The spin-up is observed for all conditions in which the tearing mode is not excited, including static and ctr-rotating. The gain in rotation depends on about the third power of the DED current as one can see in figure 6.

What is most remarkable is the direction of rotation. Without a tearing mode, the rotation is always in the direction of the plasma current (co-direction), independent of whether the DED field rotates or whether it is static. The sense of rotation is the one expected from considerations on the force transfer [20–22]. In these predictions, the ponderomotive force transfer was calculated from the induced currents at the singular surface. Since the velocity spin up extends

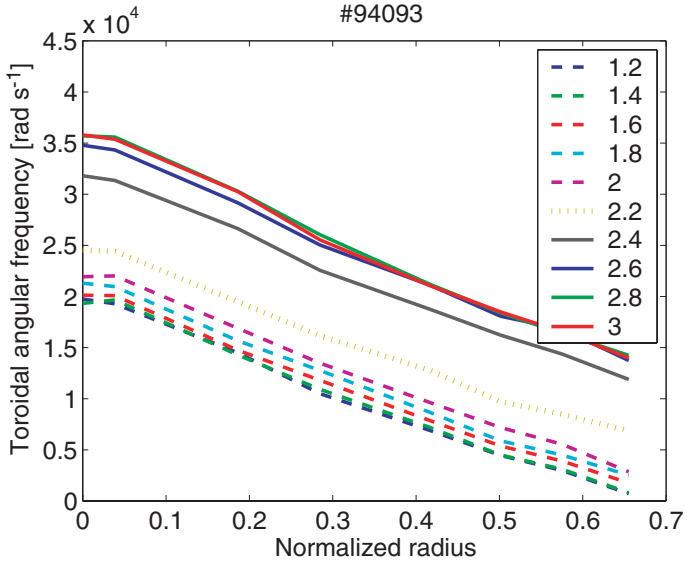

Figure 5. Profiles of the toroidal velocity measured by CXRS. For otherwise constant conditions, the co-rotating DED current is ramped up starting at 1 s, reaching its maximum at 2.5 s, keeping the amplitude constant to 3 s and ramping down to 3.2 s. The numbers in the legend are the times of the profile recordings.

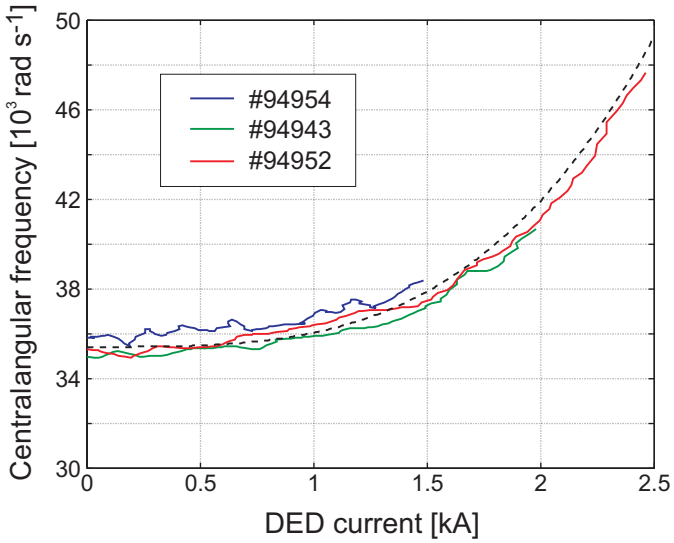

Figure 6. Toroidal velocity as a function of the co-rotating DED current.

to the edge of our measurement regime, i.e. beyond the radial locations of the resonances, there must exist another mechanism that overlays the ponderomotive force. In our tentative interpretation, we attribute the gain in toroidal velocity to a change in the electric field at the plasma edge. For a velocity change of about $10^4\,\mathrm{m\,s^{-1}}$, the term $\Delta E_\mathrm{r} = v_\mathrm{tor} * B_\mathrm{pol}$ requires a radial electric field strength of $2000\,\mathrm{V\,m^{-1}}$. The electric field would be generated by the ambipolar

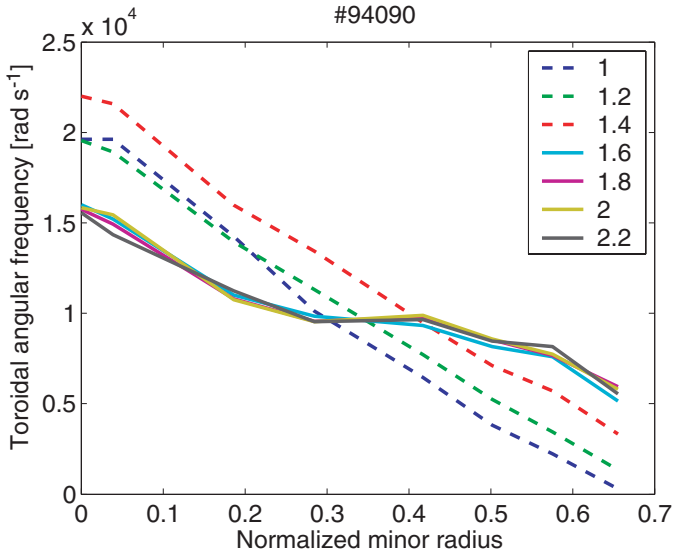

Figure 7. Velocity profile development during the onset of the $m/n = 2/1$ tearing mode. The top three curves (- - - -) correspond to the time before the mode onset and the four flat ones after the mode onset. After the onset of the tearing mode, the velocity profile is essentially flat between the $q = 1$ and the $q = 2$ surfaces. The location of the $q = 2$ surface is indicated by the horizontal green bar at $\rho = 0.6$.

plasma flow along the open magnetic field lines, where the ergodicity enhances the number of field lines intersecting the wall. This picture gives the correct sense of plasma rotation.

5. The influence of the tearing mode

If the spatial Fourier component of the DED, static or ctr-rotating, radial magnetic field $B_{m,n} = B_{2,1}$ exceeds a threshold value of about 10^{-3} T at its resonant surface, the plasma develops a tearing mode with the mode number $m/n = 2/1$ [**?**, 23–26]. The exact value of the threshold varies by a factor of two, depending on the plasma density, the heating power and heating scenario. For high plasma currents, i.e. for $q(a) < 4.5$, the plasma disrupts after the onset of the tearing mode, sometimes with a delay. At $q(a) > 5$, the discharge coexists with the tearing mode. This is a suitable scenario to investigate tearing mode physics for well reproducible conditions. If the Fourier component $B_{3,1}$ of the DED exceeds a value of about 4×10^{-3} T at the $q(r = 3)$ surface, a $m/n = 3/1$ tearing mode is excited, in addition, which coexists with the first mode. The current in the DED coils is a factor of 3–4 higher for obtaining the 3/1 tearing mode. Due to the current limitation of the power supplies, this condition can only be reached with the static DED. The tearing modes are locked to the external DED field, i.e. they are static for the static DED case and they rotate for the 1 kHz ctr-rotating case.

The tearing mode onset dominates changes in the distribution of the toroidal velocity, of the confinement and of the related transport. Figure 7 shows the velocity profile development due to the onset of the $m/n = 2/1$ tearing mode for the case of a slowly increasing DC-DED field. The three curves with the steeper slope correspond to the time before the tearing mode onset and the other three curves to the time after the onset. In the first three curves one recognizes the initial spin-up of the plasma due to the ergodization. With the tearing mode onset, the profile flattens drastically; only in the very core there is an indication of a remaining slope.

It is interesting to note that, for this example, the outer CXRS channels show a higher rotation speed than before the tearing mode onset, even though the external field is static. In other discharges, the velocity of the outer channels just matches those before the tearing mode onset. However, the radial profile towards the plasma edge is not known.

The change of the velocity is rapid in the plasma core. Within the time resolution of the CXRS-camera (5 ms), the braking of the rotation in the core and the tearing mode development are simultaneous. The acceleration of the plasma, towards the edge, is delayed with respect to the central braking and develops within 50 ms. In our opinion, the development of the tearing mode and the braking of the core rotation are directly linked. The increase in the edge rotation seems less clear. It may be that the electric current flowing in the tearing mode enhances the edge ergodization and, therefore, the plasma spins up, as described in the previous section.

For the 1 kHz ctr-rotation of the DED field, the tearing mode development and the velocity pattern are rather similar to the static DED operation; however the absolute value of the toroidal velocity [19] reduces in the core from 1.6×10^4 rad s^{-1} (DC) to 1.1×10^4 rad s^{-1} (1 kHz) and at the outermost CXRS channel from 0.6×10^4 rad to 0.2×10^4 rad s^{-1}. The edge spin up of the plasma is less strong.

At 3.5 kHz ctr-rotation of the DED field, the velocity profile changes more dramatically after the tearing mode onset than in the previous cases: the toroidal velocity reverses sign with the highest absolute value in the plasma core. The inversion of the velocity pattern is slower than described previously and requires about 100 ms. The discharge does not survive the strong change in the velocity profile and terminates a few hundred milliseconds after the tearing mode onset.

One fascinating topic is the reduction or suppression of the tearing mode excited by the DED by means of ECRH/ECCD. These studies were performed very successfully but go beyond the scope of this article. They are treated in detail by Farshi *et al* [27]. The $2/1$ tearing mode has been suppressed by 800 kW of ECRH or co-ECCD. When the mode has been suppressed by ECRH and the DED current is switched-off during the phase of mode suppression, the mode does not reappear after the ECRH pulse. Although complete suppression of the $2/1$ tearing mode has only been obtained with co-ECCD, more detailed analysis is required to assess the relative merits of localized current drive and heating. Modulated co-ECCD centred at the O-point is seen to be more effective than CW current drive at the same power, whereas modulation centred at the X-point is less effective than CW current drive at the average power.

6. Confinement and transport

For cases of pure ergodization, without tearing mode excitation, the content of the kinetic energy in the plasma is only marginally affected. Figure 8 shows the energy for two discharges, one with ergodization only and one with tearing mode. The energy measurement from the diamagnetic effect is not reliable because of electrical noise pick-up from the compensated loop. The energy is therefore derived from the profiles of electron density, electron and ion temperature. At the highest ergodization level, there is a slight tendency for the density to increase during the DED phase, which may be related to an improved particle confinement. In some discharges, the ion temperature increases slightly. However, these changes are of the 5% level. For the high confinement RI discharges [28] one sees no noteworthy change in confinement. Equally, there is also no deterioration.

In contrast to the gradual changes during the ergodization phase, the formation of a tearing mode onset decreases the stored kinetic energy immediately. The drop of the energy confinement is expected for tearing mode dominated discharges. The drop of stored energy

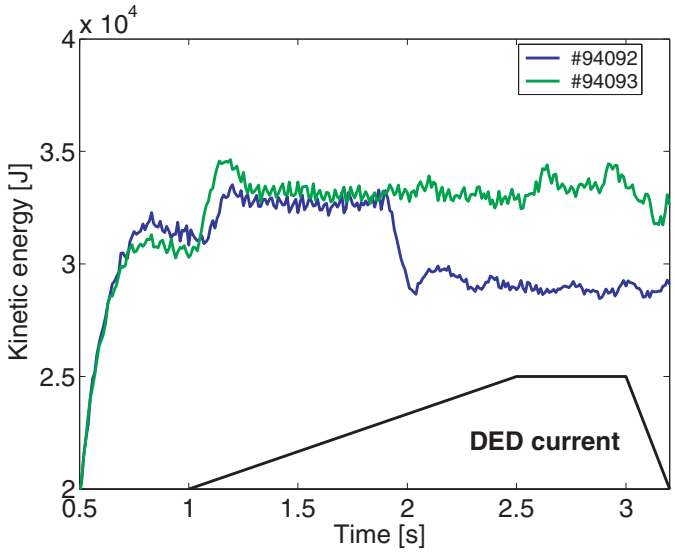

Figure 8. Kinetic energy of the plasma as a function of time for an ergodization dominated discharge (green) and a discharge with development of a tearing mode (blue). The time trace of the DED current is shown by the bottom curve. The discharge reaches steady-state density at 1.2 s.

by 15–20% is not dramatic. Since the electron density and heating power are kept constant, the kinetic energy is a direct measure of the energy confinement time.

For analysis of the local energy transport, in discharges with DED, a heat pulse analysis technique has been applied on TEXTOR. Modulation of electron cyclotron resonance heating (ECRH) is particularly suited to this because the power deposition is well localized. Also, the position of the power deposition (r_{dep}) can be chosen, by adapting the magnetic field or by applying steerable mirrors. A periodic perturbation is applied, which allows Fourier analysis of the time traces. The periodic perturbations of each time trace of the temperature are transformed into a phase (ϕ) and amplitude (A). The gradients of the ϕ and A profiles are directly related to the underlying diffusion coefficient. 'Flat' profiles in A and ϕ mean a high radial heat conductivity while a 'steep' profile indicates a reduced conductivity. Figure 9 shows different examples of the amplitude of the modulation. The top set of curves represent the Fourier amplitude A, as a function of the normalized radius, for a case where the tearing modes are avoided (co-rotating DED). The bottom set of curves is the one with the $m/n = 2/1$ tearing mode present. The red curves represent the reference scenarios without DED and the blue curve that with the highest DED current. The green curve is for medium DED current. From the steepening and flattening of the curves with respect to the reference scenario it becomes obvious that the DED action reduces the radial heat transport as long as the tearing mode is avoided. It is remarkable that the reduction of heat pulse transport is not reflected in the stored energy of the plasma (figure 8). If a tearing mode is excited, it strongly enhances the radial transport. This observation is anticipated from the reduction of the stored energy. A preliminary analysis indicates that in the ergodization dominated case the reduction of $\chi_{\mathrm{heat\text{-}pulse}}$ amounts to a factor of about 2 while the enhancement in $\chi_{\mathrm{heat\text{-}pulse}}$ with the tearing mode is about 2–4. In this respect, one has of course to keep in mind that $\chi_{\mathrm{heat\text{-}pulse}}$ represents the incremental value, which is not equivalent to the stationary heat conduction.

Even though the tearing mode excitation enhances the heat pulse and static transport, it was found that it is also connected with a transport barrier at the edge of the plasma [29].

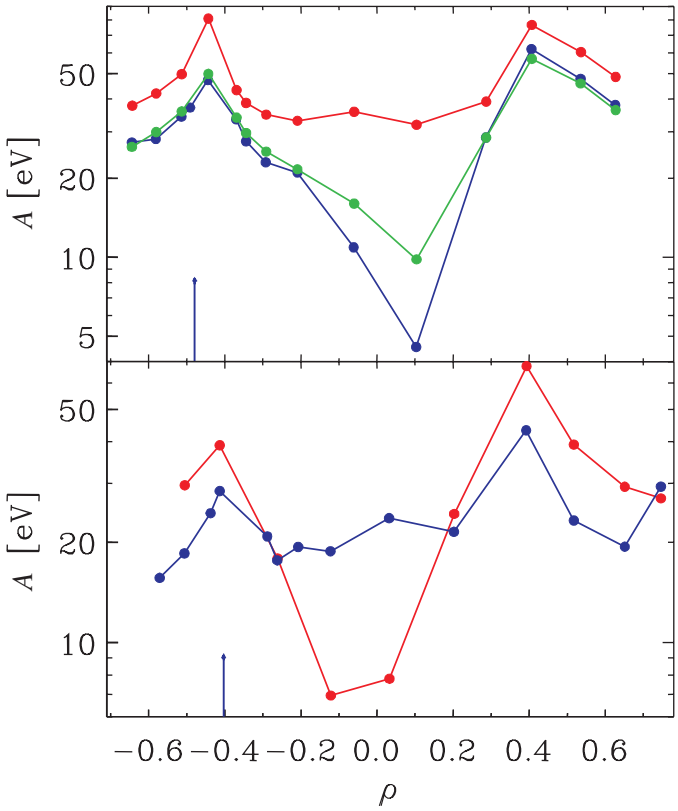

Figure 9. Analysis of heat pulse propagation induced by ECRH modulation; the ECRH is absorbed at the HFS at normalized radii $\rho = -0.5$ and 0.4 (upper and lower panel, respectively). 'A' is the amplitude of the first harmonic of the Fourier transform of T_e as measured by ECE. The red curve is without DED and the blue curve with highest DED current. The top set of curves corresponds to the ergodization dominated scenario, while the lower one to the case with tearing mode excitation.

The barrier is located around the $q = 3$ surface at $R = 2.17$ m; at this radius, the level of the phase fluctuation is decreased. The barrier cannot compensate for the enhanced power loss due to the tearing mode but it seems to ameliorate it.

Impurity transport has been analysed for the case with tearing mode excitation. For the investigations, short puffs of argon and neon were injected. Characteristic changes in the time response of several Ar ionization stages as measured by VUV-spectroscopy were observed, following the onset of a 2/1 tearing mode [30]. Two distinctive features were found: the inward motion of argon particles is considerably delayed during the onset of the tearing mode. At the same time, the central, core transport is enhanced. This observation is supported by simultaneous steady-state CXRS measurements of C^{+6} and Ne^{+10} densities. During the tearing mode the core impurity concentrations are significantly reduced whereas the lower ionization stages (CII, CIII) remain constant (impurity screening effect). Analysis of core transport coefficients, as extracted from density gradients, show that in the outer core region ($0.5 < \rho < 0.7$) the v/D ratio is reduced compared to the mode-free case. Whereas the kinetic energy content (electron- plus ion-pressure), or core energy confinement, is only moderately reduced in the presence of the 2/1-tearing mode, the plasma purity is significantly improved.

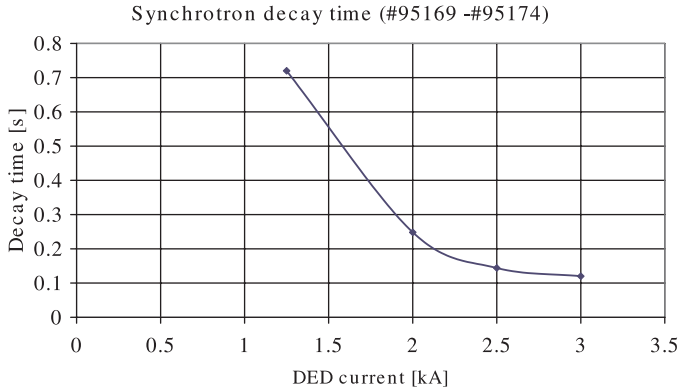

Figure 10. Runaway electrons have been used to probe the transport of energetic particles along the magnetic field lines. Also shown is the decay time of the synchrotron radiation produced by the runaway electrons.

In TEXTOR, low density discharges can be established reproducibly, with runaway electrons reaching energies of 25 MeV or more. These electrons emit synchrotron radiation at a wavelength of a few micrometres, which is detected by the IR-camera, otherwise used for thermography. Since these fast electrons are more sensitive to magnetic perturbations than to electrostatic ones, we use them for probing the particle losses of an ergodized magnetic field. We start the discharge at an electron density of 6×10^{18} m^{-3} and let the synchrotron radiation develop up to $t = 3$ s; between 3 and 4 s we switch on the static DED field for a set of currents of interest. For the rest of the discharge, the density is raised to 4×10^{19} m^{-3} by injection of helium; the collision of the runaways with the dense background plasma is sufficient to slow them down before they can create damage at the walls when the discharge terminates. Figure 10 shows the decay time of the synchrotron radiation after switching on the DED field. As expected, the runaway decay time decreases strongly with increasing ergodization level. The runaway loss starts immediately after the onset of the ergodization with the time scale shown in the figure. However, the loss is not complete and, depending on the ergodization level, the synchrotron radiation can stabilize or even increase again due to acceleration of the remaining electrons by the loop voltage. If a DED current threshold is exceeded, one observes mode activity in runaway discharges as well. In contrast to 'normal' discharges, multiple MHD events are observed, each leading to an additional loss of runaways.

7. Conclusions and outlook

In this paper, the properties of the dynamic ergodic divertor operating in the $m/n = 3/1$ configuration have been presented. The DED influences the plasma in three distinct ways: (a) the near field establishes a helical divertor; (b) the ergodization, which may be related to an edge electric field spins up the plasma rotation and improves the electron transport locally; and finally (c) the long range magnetic field perturbation is able to excite a tearing mode inside the plasma. The unique and rather reproducible plasma conditions have triggered a series of fundamental research topics. The dynamic properties of the DED have proven to be essential for reaching states that are either ergodization dominated or tearing mode dominated.

In the near future, the connections of the DED will be rearranged such that the $m/n = 12/4$ configuration will be applied at the full performance of the DED. Future topics of research will include the investigation of the difference between the coarse $m/n = 3/1$ configuration

and the relatively fine $m/n = 12/4$ set-up, which will penetrate much less into the plasma but which allows a four times higher DED-current. It is, therefore, expected that the DED will act preferentially on the plasma edge and less on the core. In the future, we will also prepare the $m/n = 6/2$ configuration, which may be an interesting intermediate between the edge limited 12/4 configuration and the long range $3/1$ set-up.

References

[1] Grosman A *et al* 1990 *Plasma Phys. Control. Fusion* **32** 1011
[2] Grosman A *et al* 1990 J. Nucl. Mater. **176–177** 493
[3] Evans T E *et al* 1992 *J. Nucl. Mater.* **196–198** 421
[4] McCool S C *et al* 1990 *Nucl. Fusion* **30** 167
[5] Evans T E *et al* 1986 *J. Nucl. Mater.* **145–146** 812
[6] Evans T E *et al* 1989 *J. Nucl. Mater.* **162–164** 636
[7] Abdullaev S S, Eich Th and Finken K H 2001 *Phys. Plasmas* **8** 2739
[8] Finken K H, Eich T and Kaleck A 1998 *Nucl. Fusion* **38** 515
[9] Finken K H, Abdullaev S S, Kaleck A and Wolf G H 1999 *Nucl. Fusion* **39** 637
[10] Eich T, Reiser D and Finken K H 2000 *Nucl. Fusion* **40** 1757
[11] Runov A M, Reiter D, Kasilov S V, Heyn M F and Kernbichler W 2001 *Phys. Plasmas* **8** 916
[12] Kobayashi M *et al* 2002 *Contrib. Plasma Physics* **42** 163
[13] Abdullaev S S *et al* 2003 *Nucl. Fusion* **43** 299
[14] Giesen B *et al* 1997 *Fusion Eng. Des.* **37** 341
[15] Finken K H 1997 *Nucl. Fusion* **37** 583
[16] Finken K H, Abdullaev S S, Jakubowski M, Lehnen M and Sewell G 2004 *Nucl. Fusion* **44** S55
[17] Liang Y *et al* 2004 *31st European Conf. on Plasma Physics (London)* P1-125
[18] Lehnen M *et al J. Nucl. Mater.* at press
[19] de Bock M *et al* 2004 *31st European Conf. Plasma Physics (London)*
[20] Finken K H 1999 *Nucl. Fusion* **39** 707
[21] Pankratov I M, Omelchenko A Ya, Olshansky V V and Finken K H 2004 *Nucl. Fusion* **44** S37
[22] Elfimov A G *et al* 2004 *Nucl. Fusion* **44** S83
[23] Koslowski H R *et al* 2004 *31st European Conf. on Plasma Physics (London)* P1-124
[24] Liang Y *et al* 2004 *31st European Conf. on Plasma Physics (London)* P1-125
[25] Zimmermann O *et al* 2004 *31st European Conf. on Plasma Physics (London)* P1-129
[26] Varshney S K *et al* 2004 *31st European Conf. on Plasma Physics (London)* P1-127
[27] Farshi E *et al* 2004 *31st European Conf. on Plasma Physics (London)* P1-122
[28] Van Wassenhove G *et al* 2004 *31st European Conf. on Plasma Physics (London)* P1-129
[29] Krämer-Flecken A *et al* 2004 *31st European Conf. on Plasma Physics (London)* P1-120
[30] von Hellermann M G *et al* 2004 *31st European Conf. on Plasma Physics (London)* P1-118